Paleoceanography and Paleoclimatology

RESEARCH ARTICLE
10.1029/2021PA004290

ENSO's Response to Volcanism in a Data Assimilation-Based Paleoclimate Reconstruction Over the Common Era

Sylvia G. Dee[1] **and Nathan J. Steiger**[2,3]

[1]Department of Earth, Environmental, and Planetary Sciences, Rice University, Houston, TX, USA, [2]Institute of Earth Sciences, Hebrew University, Jerusalem, Israel, [3]Lamont-Doherty Earth Observatory, Columbia University, Palisades, NY, USA

Key Points:

- The relationship between ENSO and volcanic eruptions is tested in a new paleoclimate data assimilation product, PHYDA, spanning 1–2000 CE
- A weak El Niño-like warming emerges in frequency-based analyses, but not when using commonly employed superposed epoch analysis
- Comparisons between GCMs and paleoclimate data using frequency analyses such as self-organizing maps could reduce data–model discrepancies

Supporting Information:

Supporting Information may be found in the online version of this article.

Correspondence to:

S. G. Dee,
sylvia.dee@rice.edu

Citation:

Dee, S. G., & Steiger, N. J. (2022). ENSO's response to volcanism in a data assimilation-based paleoclimate reconstruction over the Common Era. *Paleoceanography and Paleoclimatology*, *37*, e2021PA004290. https://doi.org/10.1029/2021PA004290

Received 20 APR 2021
Accepted 8 FEB 2022

Author Contributions:

Conceptualization: Sylvia G. Dee, Nathan J. Steiger
Data curation: Sylvia G. Dee
Formal analysis: Sylvia G. Dee
Funding acquisition: Sylvia G. Dee, Nathan J. Steiger
Investigation: Sylvia G. Dee, Nathan J. Steiger
Methodology: Sylvia G. Dee, Nathan J. Steiger
Project Administration: Sylvia G. Dee, Nathan J. Steiger
Resources: Sylvia G. Dee, Nathan J. Steiger
Software: Sylvia G. Dee, Nathan J. Steiger
Supervision: Sylvia G. Dee

Abstract The tropical response to explosive volcanism remains underconstrained in the paleoclimate record. While the atmosphere cools due to aerosol forcing following volcanic eruptions, modeling evidence suggests that the tropical Pacific responds with compensatory warming. Given the rarity of large volcanic eruptions and the short instrumental record, these modeling results require independent verification. Here, we test for links between volcanism and tropical Pacific dynamics using the newly developed Paleo Hydrodynamics Data Assimilation product (PHYDA), which spans the past 2,000 years. Using Pacific sea surface temperature fields from PHYDA and coincident volcanic eruptions, we test the response of the El Niño–Southern Oscillation (ENSO) to large, tropical volcanic eruptions. We identify a weak El Niño-like response of the tropical Pacific in the year following sufficiently large, tropical volcanic eruptions. While the response is not significant at the 95% confidence level using superposed epoch analysis (SEA) and self-organizing maps, a significant result does emerge when employing probability density functions. Our results indicate that the widely used SEA approach, based on composite averaging, may not be sufficiently sensitive to capture an ENSO response in the presence of large internal variability. We additionally conclude that inconsistencies in both the spatial patterns and magnitudes between climate models and PHYDA results indicate that current models overestimate the regional tropical response to volcanic forcing.

1. Introduction

Despite its bearing on global climate variability, some important aspects of El Niño–Southern Oscillation (ENSO)'s response to external forcing and the underlying physics remain controversial (e.g., Dee et al., 2020). In particular, there is conflicting evidence for whether or not ENSO dynamically responds to the radiative forcing of large volcanic eruptions. During periods of explosive volcanism, sulfate aerosols are injected into the stratosphere and scatter incoming solar radiation, causing short-term (1–5 years) global cooling between −0.1°C and −0.5°C (Angell, 1988; Angell & Korshover, 1985; Handler & Andsager, 1994; McCormick et al., 1995; Robock & Mao, 1995; Shindell & Schmidt, 2004; Shindell et al., 2003, and see Robock, 2000, for a review). Coupled climate models simulate a robust cooling response to volcanic forcing (Church et al., 2005; Gleckler et al., 2006; Stevenson et al., 2016; Timmreck, 2012); both temperature and precipitation decrease following the Pinatubo eruption in observations and the Atmospheric Model Intercomparison Project 5 (AMIP5) multimodel ensemble, for example (Meyer et al., 2016).

To date, a number of studies have hypothesized and tested the potential for a causal relationship between explosive volcanism and El Niño events. Previous studies using both paleoclimate data and coupled general circulation models (GCMs) have suggested that volcanic eruptions might cause, or increase the likelihood of, El Niño events or an "El Niño-like" state (Adams et al., 2003; Emile-Geay et al., 2008; Handler, 1984; Khodri et al., 2017; Maher et al., 2015; Pausata et al., 2015, 2016; Stevenson et al., 2016). For example, Stevenson et al. (2016) investigate the response to last millennium volcanism in the Community Earth System Model (CESM) last millennium ensemble (LME) and find that El Niño events are more likely to occur during the two boreal winters following an eruption, accompanied by a slowing of the Walker circulation. Warming resembling the spatial features of El Niño occurs in the winter of posteruption years 1 and 2, with a decreased probability of La Niña conditions (Stevenson et al., 2016). These responses were found statistically significant for all eruptions in the full ensemble; but, CESM ENSO variance exceeds that of the observations by a factor of 2, and this enhanced ENSO response may amplify interactions with volcanic cooling (Stevenson et al., 2016).

Validation: Sylvia G. Dee, Nathan J. Steiger
Visualization: Sylvia G. Dee
Writing – original draft: Sylvia G. Dee, Nathan J. Steiger
Writing – review & editing: Sylvia G. Dee, Nathan J. Steiger

The *ocean dynamical thermostat mechanism* provides a dynamical hypothesis linking volcanic cooling and ENSO (Clement et al., 1996; Emile-Geay et al., 2008): reduced solar radiation due to volcanic aerosol scattering preferentially cools the western equatorial Pacific, shoals the zonal tropical Pacific sea surface temperature (SST) gradient, and weakens the trade winds. This in turn promotes El Niño conditions (Clement et al., 1996), and the eastern equatorial Pacific warms to compensate for cooling. However, it has been suggested that only large, explosive tropical eruptions increase the likelihood of or generate an El Niño event, whereas smaller eruptions do not create a significant effect (Adams et al., 2003; Emile-Geay et al., 2008; Mann et al., 2005). The role of internal variability (Emile-Geay et al., 2008; Lehner et al., 2016), subtropical wind stress (McGregor & Timmermann, 2011), the migration of the Intertropical Convergence Zone (ITCZ; Pausata et al., 2015), or continental cooling (Ohba et al., 2013) may all contribute to a complex and multifaceted tropical Pacific response to volcanism.

The nature of the connection between ENSO and volcanism has been further explored using paleoclimate data, primarily using tree-ring width (TRW) records. Stevenson et al. (2016) show that the hydroclimate response to volcanism in CESM disagrees with TRW data from North America and Southeast Asia (Anchukaitis et al., 2010; Li et al., 2013). However, Adams et al. (2003) examined two TRW paleoclimate reconstructions (with a record extending back to 1649) and showed that volcanism and the associated global cooling roughly doubled the likelihood of an El Niño event by nudging the ocean–atmosphere system toward a state where El Niño conditions are favored. The authors found a significant, multi-year, El Niño-like response to explosive tropical forcing using two independent reconstructions of El Niño spanning the past several centuries, and demonstrated a doubling of the probability of a wintertime El Niño event if a low-latitude volcanic eruption occurs in the previous year. Furthermore, the authors suggest that there is a subsequent rebound into La Niña conditions following this change, meaning that volcanic eruptions effectively synchronize the internal clock of ENSO. However, recent high-resolution coral reconstructions from Palmyra Atoll stand in contrast to these studies and do not show a significant ENSO response to volcanic eruptions during the last millennium (Dee et al., 2020).

Though recent work has made progress toward resolving such discrepancies via investigations of proxy biases (Zhu et al., 2020), ENSO's response to volcanism remains inconsistent in model simulations and the paleoclimate record. A clear, consistent diagnosis of the causal mechanism, if any, between volcanism and ENSO is lacking (and see Emile-Geay et al., 2020, for a review). The primary barrier to a full diagnosis of ENSO's response to such external forcing is the lack of long-term reconstructions of ENSO dynamics that could be analyzed along with the volcanic forcing record. There are a large number of studies that have used paleoclimate data (Adams et al., 2003; Anchukaitis et al., 2010; Dee et al., 2020; Li et al., 2013; Stevenson et al., 2016) and model simulations (as described above) to evaluate ENSO's response to volcanism. Extending this, several recent papers explore the tropical Pacific response to external forcing in new data assimilation products, including the Last Millennium Reanalysis (LMR, Sanchez et al., 2021; Tardif et al., 2019; Zhu et al., 2022) and the Paleo Hydrodynamics Data Assimilation product (PHYDA; Steiger et al., 2018). While two recent papers explore the global hydroclimate (Tejedor et al., 2021a) and temperature responses (Tejedor et al., 2021b) to volcanic eruptions in PHYDA, in general, no studies to date have focused primarily on the dynamical response of ENSO to volcanism in this paleoclimate data assimilation reconstruction.

To this end, here, we expand on previous work to investigate the tropical Pacific response to volcanism in the PHYDA, which is a seasonally resolved paleoclimate data assimilation product spanning the last 2,000 years (Steiger et al., 2018). PHYDA allows us to test the predominant theory for the tropical Pacific response to volcanism within a framework that naturally includes information from both climate models and paleoclimate data. The temporal and global spatial coverage of PHYDA facilitates examination of the timing of warming and cooling events proximal to volcanic eruptions. PHYDA's 2,000-year long reconstruction of NIÑO-region SSTs additionally provides roughly ∼1,000 years of additional overlap with the most recent volcanic forcing reconstructions from Toohey and Sigl (2017), which date back to 500 BCE; this expands the number of eruptions in our analysis compared to studies which focus solely on the last millennium (e.g., Dee et al., 2020; Stevenson et al., 2016; Zhu et al., 2020). PHYDA thus provides a complimentary paleoclimate test bed for comparison against the climate model response to tropical volcanism.

If a mechanism linking external forcing to ENSO variability exists, such a relationship should be resolved in state-of-the-art paleoclimate data assimilation products such as PHYDA. Given that spatial patterns of ENSO SSTs are highly variable (Capotondi et al., 2015; Johnson, 2013), our approach employing a full spatiotemporal

SST grid can provide further tests of the null hypothesis that volcanism favors an El Niño-like response. Unlike paleoclimate reconstructions derived from point-based data from corals or networks of tree rings, PHYDA incorporates all available paleoclimate data with climate model physics to provide a reconstruction of the entire spatial field for each year in the last 2,000 years. This gives us the opportunity to examine not only the reconstructed magnitude of the SST response but also the *pattern* of SST changes following a volcanic eruption. (However, note that the spatial SST patterns present in PHYDA are based on the underlying climate model used in the creation of PHYDA.) Furthermore, evaluation of the full SST field facilitates direct comparison to climate model simulations, which provide detailed spatial information on both the magnitude and patterns of SST changes during ENSO events.

In tandem with reconstructions of volcanic aerosol reconstructions spanning the last 2,000 years, we use PHYDA's reconstruction of NIÑO region SSTs (Section 2) and evaluate the response to volcanic forcing using three different methods: superposed epoch analysis (SEA), probability density functions, and self-organizing maps (SOMs; Section 3). Implications for the robustness of volcanic impacts on ENSO, as well as the sensitivity of our results to the analysis method employed, are discussed in Section 4.

2. Data and Methods

2.1. PHYDA

The recently developed PHYDA is the first global reconstrfuction of temperature, hydroclimate, and dynamical variables over the past 2,000 years (Steiger et al., 2018). It is based on paleoclimate data assimilation, which optimally combines paleoclimate proxies with the dynamical constraints of coupled climate models. In particular, PHYDA assimilated 2,978 proxy data time series to produce probabilistic annual, seasonal, and monthly reconstructions of the past 2,000 years (Figure 1a). (For this study, we employ annually averaged fields only.) PHYDA's underlying proxy network varies in time, with reductions from the full network such that there are approximately 650 proxies by the year 1500, 200 proxies by the year 1000, 100 proxies by the year 500, and 50 proxies by the year 1 (see Steiger et al., 2018; Figure 1).

PHYDA has been extensively validated in both the original publication (Steiger et al., 2018) as well as subsequent uses, showing in particular that PHYDA has a more realistic ENSO than the underlying model used in its construction (Steiger et al., 2019). PHYDA's cooling response to volcanic eruptions is very similar to maximum late-wood density tree-ring reconstructions despite the DA inclusion of extensive TRW data (Tejedor et al., 2021a). Additionally, Steiger et al. (2018) showed that the ENSO region contains areas with some of the most skillful and accurate ensemble estimates for all of PHYDA's three seasonal averages. Here, we employ the annual SST fields and NIÑO3.4 index from PHYDA spanning years 1–2000 CE (Figure 1a) to test the hypothesis that El Niño events increase in frequency or severity after strong eruptions.

The model prior employed for PHYDA's data assimilation is the Community Earth System Model version 1.2 Last Millennium Ensemble (CESM-LME; Kay et al., 2015). The model prior comprises a critical component of the data assimilation reconstruction: all spatial covariance information is derived from the model prior, whereas the time history of the reconstruction is entirely driven by the underlying proxy data. Note that PHYDA's SSTs have additionally been bias corrected from the original CESM-LME output (Steiger et al., 2019).

Like most climate field reconstructions, PHYDA's uncertainties change through time as the number and quality of proxy data change. We illustrate this effect for PHYDA's NIÑO3.4 reconstruction in Figure S1 in Supporting Information S1. The supplemental figure shows the standard deviation of PHYDA's NIÑO3.4 ensemble reconstruction through time (red line) and also the standard deviation of the CESM-LME NINO3.4 index (gray dashed line), given that the CESM-LME is the data assimilation prior for PHYDA. The standard deviations have been normalized with respect to the CESM-LME simulation. For reference, we also include the mean standard deviation for all 2 m temperature grid point time series in PHYDA (black dashed line). Several important features emerge: uncertainties increase with time as more proxies are lost further back in time. In addition, Figure S1 in Supporting Information S1 shows the specific uncertainty impact of particular proxies being added and removed through time, as seen by the jumps in the time series (likely, this is driven by the presence of proximal tropical coral records). Broadly, there is no point in time where PHYDA's ensemble estimates are consistent with a no-information reconstruction, which would show PHYDA converging to the prior ensemble (here, the CESM-LME).

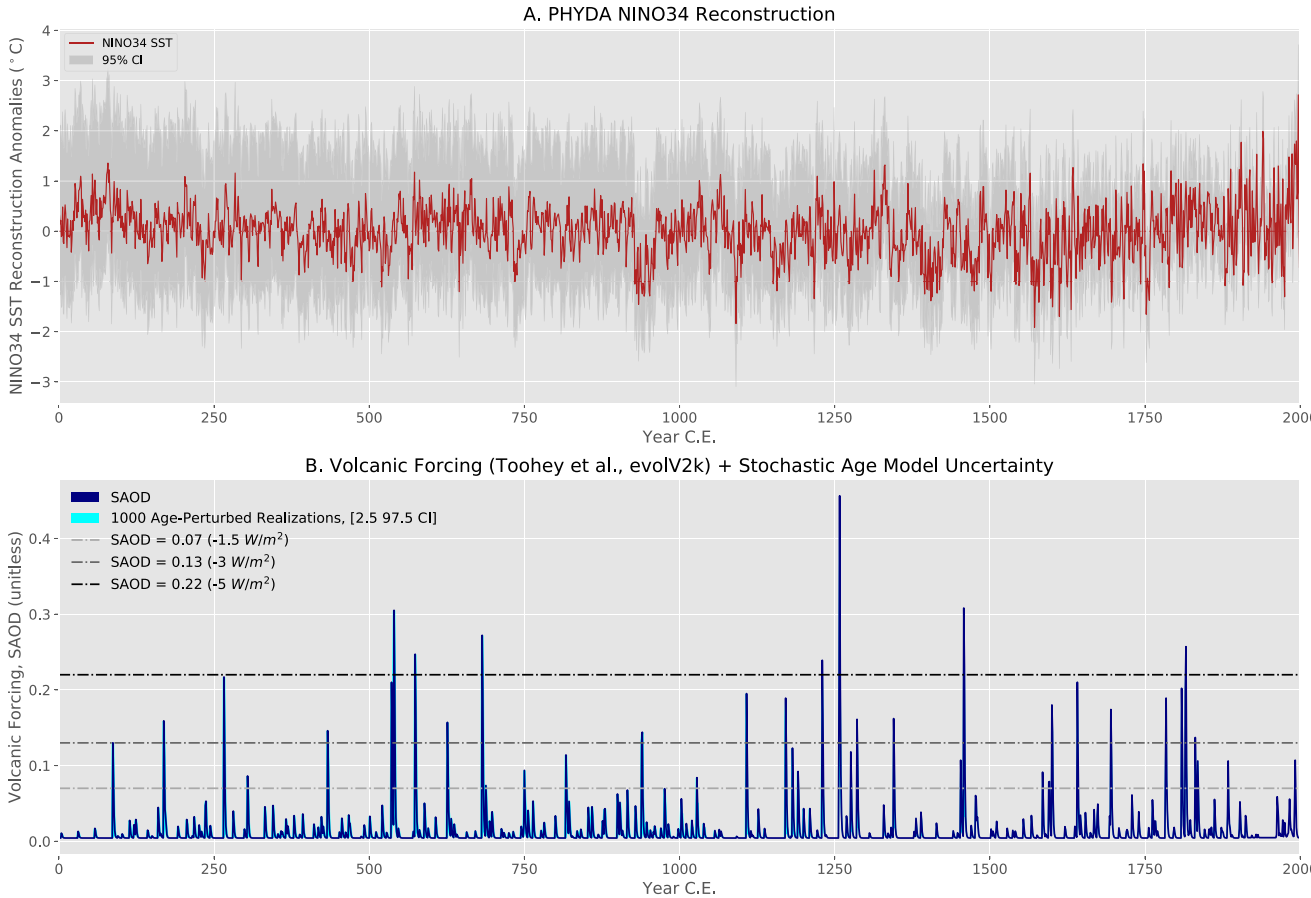

Figure 1. Reconstructed volcanism and NIÑO3.4 sea surface temperatures (SSTs) over the last millennium. (a) Reconstructed NIÑO3.4 SST index anomalies from Paleo Hydrodynamics Data Assimilation product (PHYDA; Steiger et al., 2018) (red) along with the 95% confidence interval from the PHYDA ensemble (light gray). (b) Reconstructed volcanic eruptions from the Toohey and Sigl (2017) eVolv2k data set (navy). Stratospheric aerosol optical depth (SAOD) thresholds (dashed-dot gray lines) indicate the volcanic forcing thresholds employed in analysis. Also shown are Banded Age Model-simulated stochastic age uncertainties; 95% CI given a 0.03% error rate.

In conjunction with the skillful ensemble uncertainty estimates shown in Steiger et al. (2018), Figure S1 in Supporting Information S1 thus indicates that there is useful information within PHYDA's NIÑO3.4 reconstruction over the full Common Era.

2.2. Volcanic Forcing Reconstruction

Our volcanic forcing data are taken from the eVolv2k database (Toohey & Sigl, 2017), a reconstruction of volcanic events based on multiple indicators in ice core records. Figure 1b highlights the largest eruptions of the last millennium (spanning the period 1–2000 CE) in terms of stratospheric aerosol optical depth (SAOD); all volcanic data points within the Common Era intersect the PHYDA reconstruction. Given our focus on tropical climate variability, we restrict our analysis to tropical eruptions only. Tropical eruptions are characterized by the presence of sulfate aerosols in both Arctic and Antarctic ice core records, using the assumption that high-latitude eruptions will be captured only in ice cores of their corresponding pole; sufficiently explosive and sulfurous tropical eruption ash and particulate matter advect toward both poles as a result of stratospheric circulation (Adams et al., 2003; Toohey & Sigl, 2017).

2.3. Superposed Epoch Analysis

We employ SEA (and see Adams et al., 2003; Dee et al., 2020, for a full description of the methodology) to test for a response in the NIÑO34 reconstruction following a volcanic eruption. To test for sensitivity to eruption size, we repeat the SEA for SAOD thresholds of 0.07, 0.13, 0.22, and 0.4, which correspond to radiative forcings of approximately −1.5, −3, −5, and −10 W/m^2, depending on sulfate aerosol scaling uncertainties (Toohey & Sigl, 2017); thresholds are marked in Figure 1b. (For reference, Mt. Pinatubo's 1991 emissions were estimated to produce a SAOD of 0.11). A Monte Carlo resampling test (n = 1,000 redraws) of the SST field during non-volcanic eruption years was used to test for significance of the SEA results. The block-bootstrap resampling tests against the null hypothesis that the temperature response could occur randomly, rather than a forced response.

2.4. Self-Organizing Maps

We use a SOM algorithm (Kohonen, 1998) to extract the primary modes of Pacific SSTs within PHYDA. The SOM algorithm assigns annual SST anomaly fields to spatial patterns of a preset number of "nodes" (or patterns). The method essentially creates spatial patterns that maximize their similarity with the underlying SST fields by minimizing their Euclidian distance. The algorithm then assigns each annual SST field to the best matching pattern. The SOM patterns are approximately the mean of the assigned SST fields and are thus approximately a composite of relatively similar SST fields (Johnson et al., 2008). Additionally, the SOM analysis organizes the patterns such that similar patterns are assigned to nearby locations within a regular two-dimensional grid. Thus, this full process allows one to visualize a reduced-space continuum of patterns in the data set. For the SOM analysis, the SST fields are preprocessed by detrending the SST fields. We removed the trend derived from a 100 years LOWESS smoothing of each individual grid point time series (where the detrended time series is equal to the original time series minus the smoothed time series; LOWESS computes a local regression using weighted linear least squares with a first degree polynomial). This detrending prevents spurious trends in the pattern occurrence (Horton et al., 2015), especially during the postindustrial period. Additionally, the SST data are area-weighted prior to computing the SOMs (Johnson et al., 2008). Our calculation of the SOMs uses a geographic range of 102.5°–297.5°E, 33°S–33°N, spanning only the tropical Pacific region.

2.5. Dating Uncertainties

To account for plausible dating uncertainties in the volcanic forcing reconstruction, we applied the Banded Age Model (BAM; Comboul et al., 2014) to the volcanic SAOD time series. BAM inserts errors whereby "true" dates are shuffled stochastically, provided some error rate in the age model. SAOD volcanic forcing data are reported with maximum age model errors on the order of 1–2 years (Toohey & Sigl, 2017). While this maximum dating error is unlikely due to replication and well-constrained top-dates, we nevertheless experimented with two age models: (a) using BAM, we assume stochastic age model errors such that years are dropped or doubly counted so that the total error is approximately 2 years max; (b) we assume the entire chronology is shifted as a unit ±1–2 years. The volcanic eruption dates are therefore randomly shifted by 1–2 years maximum, and 1,000 new chronologies are generated by the model. We subsequently tested these two age model scenarios alongside the "true" or "original" age model, which assumes a perfect temporal constraint.

2.6. Uncertainty Quantification

For both the SEA and SOM analyses, we perform standard resampling tests to check for significant changes in tropical Pacific SST during eruption years, applying a 95% confidence level to establish significance. Changes in the SEA SST patterns and shifts in the SOM pattern frequencies are compared to a background of all years in the PHYDA ensemble. The three methods employed here (SEA, probability density functions, and SOMs) all apply different tests to establish statistical significance. For the SEA, we use a block-bootstrap resampling of the full ensemble spread. The probability density function shifts are evaluated using a two-tailed t test. For the SOMs, we resample n eruption years at random, m = 1,000 times, for all years compared to the "true" eruption years. We additionally resample the ensemble of age-perturbed chronologies (Section 2.5, Figure 1). Essentially, we test for

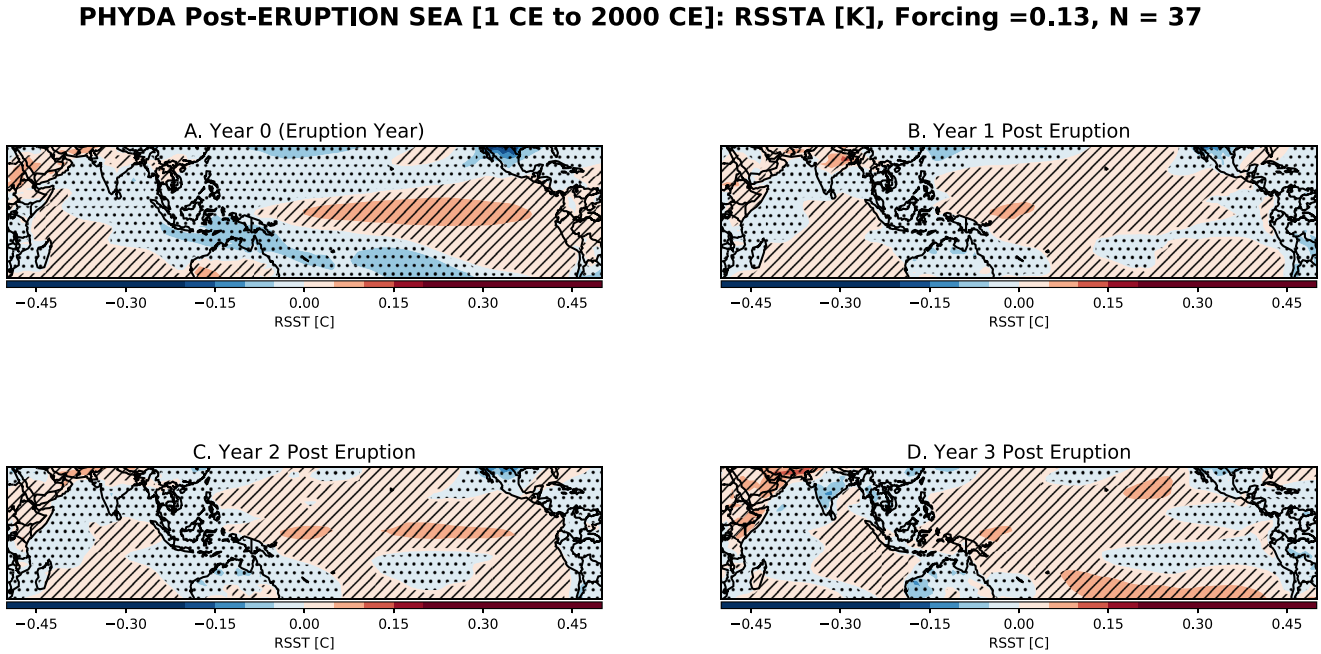

Figure 2. Superposed epoch analysis composite maps for volcanic forcing (SAOD > 0.13, $n = 37$ eruptions). Nine-year windows are extracted from the tropical relative SST data, centered about volcanic eruptions generating radiative forcing for the given threshold. Year 0 is the eruption year. Data shown are the composite averages across all eruption horizons. Red colors indicate warmer conditions, and blue colors indicate cooler conditions surrounding eruptions. Hatching or stippling indicates that the response to volcanic forcing is not significant at the 95% confidence level.

significant shifts against a background state composed of all years using a resampling methodology to account for random uncertainties.

3. Tropical Response to Volcanic Forcing

Volcanic aerosol forcing reduces the amount of energy available to the atmosphere, resulting in cooling; this should in turn result in less precipitation and weakening circulation, both in the trade winds and Walker Circulation (e.g., Meyer et al., 2016). These energetic changes may impact ENSO characteristics for sufficiently large volcanic events. We here define and test the null hypothesis (H0): *significant changes in ENSO variability follow sufficiently explosive volcanism*. H0 is tested using annual tropical Pacific SST indices for ENSO activity and annual spatial fields of SST from PHYDA. Note that the annual average in PHYDA is copu April to the next calendar year March, capturing the hydrological year. Figure 1b shows 2,000 years (1–2000 CE) of the Toohey and Sigl (2017) volcanic forcing reconstruction plotted alongside the PHYDA NIÑO3.4 reconstruction, Figure 1a, which are analyzed together in the results that follow.

3.1. Pacific SST Composite Pattern Response

We used SEA (Methods) to test for a response in reconstructed tropical SST following a volcanic eruption. We apply multiple thresholds for volcanic eruptions exceeding SAOD > 0.07, 0.13, 0.22, and 0.4 (Figure 1b and Figures S2–S4 in Supporting Information S1), which capture the largest 74, 37, 9, and 1 eruptions within the period 1–2000 CE, respectively. SEA is applied to the full SST field for all eruption years and composited to detect a coherent response. Note that this analysis uses relative SST, wherein the tropical mean (20°S–20°N) is removed to separate the ENSO signal from tropics-wide volcanic cooling (as in Khodri et al., 2017). Figure 2, which shows the response for eruptions with SAOD > 0.13, shows that in the eastern and central tropical Pacific, SSTs weakly shift toward warmer conditions (on the order of ~0.1°C–0.15°C) in the 2 years following the eruption (Figure 2, top panel). By year 3, warming in the western Pacific and weak cooling across the eastern equatorial Pacific emerge. A block-bootstrap resampling of the PHYDA ensemble data indicates that the relatively small

SST changes in this SEA analysis are not significant at the 95% confidence level (hatching on figure indicates lack of significance).

To test for sensitivity in the SST response to eruption size, we performed an identical SEA for SAOD thresholds of 0.07, 0.22, and 0.4, which correspond to radiative forcing of approximately −1.5, −5, and −10 W/m^2, respectively (Toohey & Sigl, 2017; Figures S2–S4 in Supporting Information S1, respectively). For the lowest forcing threshold composite (SAOD = 0.07), as in Figure 2, a muted central Pacific (or "El Niño-like") warming response occurs in years 0–2, with posteruption cooling by year 3 (Figure S1 in Supporting Information S1). For eruptions exceeding SAOD of 0.22 and 0.4, warming in the eruption year is overtaken by a relatively strong cooling response in years 1–3. We note a very small sample size for these larger eruption sizes ($n = 9$, $n = 1$, respectively). None of the SST changes are significant at the 95% level (Figures S2 and S3 in Supporting Information S1). Using the age-perturbed ensemble of volcanic forcing years, we recomputed the SEA for the 5th and 95th confidence intervals of the ensemble (Figures S7 and S8 in Supporting Information S1). The SEA performed on the age-perturbe shows no change in significance at the 95% level, and a significant cooling signal in year 3 for the 5% CI (Figure S7 in Supporting Information S1).

Finally, Figure S5 in Supporting Information S1 shows the SEA composite response of central Pacific (NIÑO3.4) SSTs in the 3 years prior and 6 years following all sufficiently large eruptions for three eruption thresholds (0.07, 0.13, 0.22). In the central Pacific, SSTs are warmer in the eruption year (0) but show no or very small changes in the following year (+1). All three SEA panels suggest a shift toward cooler SSTs in years +2 to +6. The 95% confidence intervals of 1,000 Monte Carlo block-bootstrap realizations of the data are shown in gray dashed lines. Extrapolating from the significance testing results, none of the post-eruption SEA responses are significant at the 95% level. Interestingly, the pre-eruption warming in the year prior to the eruption SAOD > 0.07 is significant (Figure S5a in Supporting Information S1), potentially indicative of a random bias toward El Niño conditions due to internal variability preceding volcanic eruptions. Additional evaluation of the SOM frequencies (Section 3.3) also indicates an increase in El Niño-like SST conditions for the year before eruptions (not shown); the relatively small eruption sample size makes this difficult to confirm, however.

Resolving the full pattern of SSTs affords spatiotemporal information capturing the tropical Pacific response to volcanism that point-based paleoclimate proxy reconstructions do not (though we note the influence of the DA prior, CESM, on the spatial pattern). The maps compositing the SST changes across the full tropical Pacific basin indicate localized warming in the central Pacific, but PHYDA's warming response (shown in Figure 2a) is small, with a maximum warming of ∼0.1°C–0.15°C. SEA on the NIÑO34 index values similarly indicate weak and insignificant warming in the eruption year, followed by a stronger cooling signal. This muted warming stands in contrast to previous modeling studies which have suggested a warming response exceeding 1°C (e.g., Pausata et al., 2016; Stevenson et al., 2016); furthermore, the warming response is not significant at the 95% level.

3.2. SST Index and Frequency Responses

As a complement to the widely used, composite averaging-based SEA analyses, we also use two frequency-based analyses. In this first frequency-based analysis, we show changes in probability density functions for annual SSTs in the NIÑO3.4 region in the year of and 2 years following volcanic events. We compared these data to the mean of all non-eruption years as a baseline (Figure 3). Figure 3 shows the composite change in the probability density functions (PDF) for the NIÑO3.4 index (Steiger et al., 2018), as well as the change in the percentiles of NIÑO3.4 SST anomalies. To capitalize on the full PHYDA ensemble, Figure 3 includes data for volcanic eruption years in all ensemble members. We evaluated the impact of eruption size on the SST response, starting with a lower eruption magnitude of SAOD > 0.07 and increasing the threshold to SAOD > 0.22. Note that for an SAOD > 0.22 (Figures 3e and 3f), only nine of the largest eruptions within the period 1–2000 CE are included in the analysis.

The PDFs, when all ensemble members are included, indicate significant shifts toward warm SSTs in the posteruption means of the PDFs ($p < 0.05$, two-tailed t test). There is an unusual increase in the frequency of warm NIÑO3.4 region anomalies during the eruption year for large events (black curves compared to gray, Figures 3a, 3c, and 3e). These results hold for all SAOD thresholds (0.07, 0.13, 0.22).

Changes in the percentiles of NIÑO3.4 region SSTs are shown alongside the PDFs in Figures 3b, 3d, and 3f. We computed the (5th, 25th, 50th, 75th, and 95th) percentiles of the NIÑO3.4 SST anomalies for the ensemble of eruption and noneruption years. As shown in Figures 3b, 3d, and 3f, SSTs are generally warmer in the eruption year

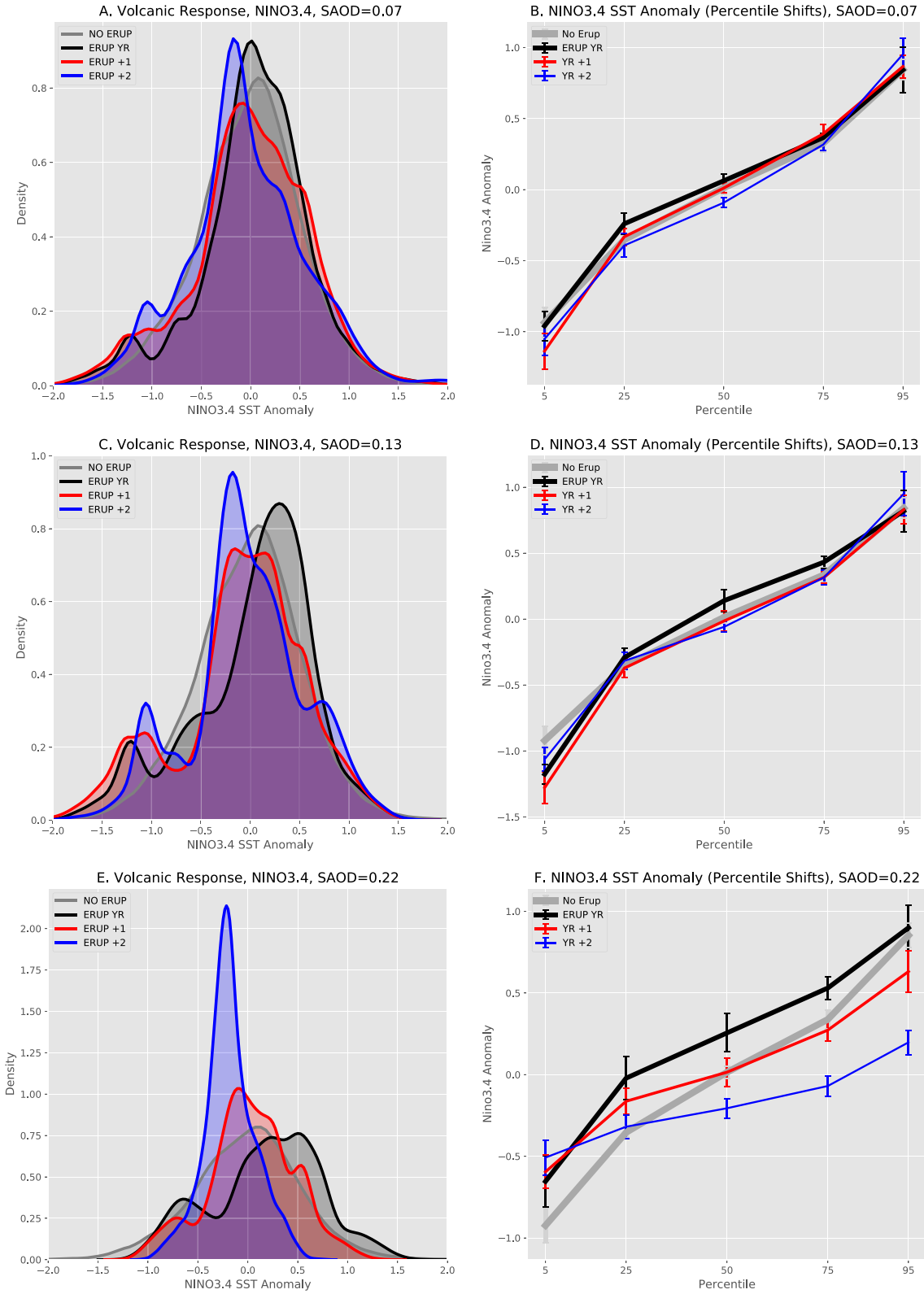

Figure 3. NIÑO3.4 index changes in response to volcanic eruptions. Probability density functions for annually averaged NIÑO3.4 index values for the 2 years following the eruption year; shown are the PDFs for the full PHYDA ensemble ($n = 998$ ensemble members) of all eruption years exceeding the SAOD threshold (0.07, 0.13, and 0.22). Plotted are the eruption year (black), YR + 1 (red), +2 (blue). Gray thick line: PHYDA ensemble mean data for noneruption years. (a, c, e) NIÑO34 region SST anomalies, PDF, for varying eruption thresholds. (b, d, f) Change in percentiles (5%, 25%, 50%, 75%, 95%) for NIÑO34 SST anomalies.

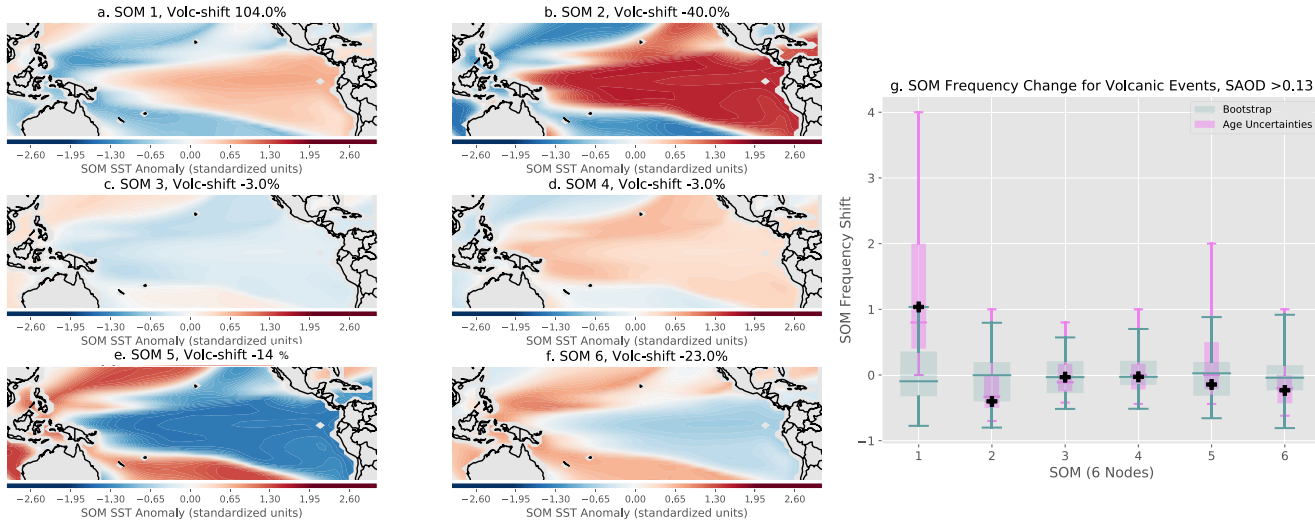

Figure 4. Self-organizing map analysis for eruptions with SAOD > 0.13. (a–f) The fundamental self-organizing map (SOM)-derived SST patterns. Each SOM is labeled with the percent change in the pattern frequency for volcanic eruption years only. The map color scale corresponds to the SOM SST anomalies in standardized units. The largest change in pattern frequency for eruption years is in pattern 1, which increases by 104%. (g) Shift in Self-Organizing Map Pattern Frequency. Changes in pattern frequency for eruption years (SAOD > 0.13) in black crosses compared to noneruption years (box plot range for n = 1,000 random draws from noneruption pattern assignments in dark cyan and from age-perturbed ensemble in purple). Frequency is computed as the occurrence of years corresponding to each pattern (node frequency) within the full pool of data.

(black curve falls above gray curve, indicating the NIÑO3.4 SST anomalies are higher for a given percentile). However, in years +1 and +2, SST anomalies are generally the same as noneruption years or colder, especially for the largest eruption class (Figure 3f). Most shifts in PDFs are significant at the 95% confidence level (based on a two-tailed t test). There is one important exception: as shown in Table S1 in Supporting Information S1, all shifts are significant at the 95% confidence level except year +1 for SAOD = 0.07 (p = 0.5). Indeed, Figure 3b shows that the red curve (YR + 1) is very similar to the no-eruption years response.

3.3. Self-Organizing Map Analysis

We employed a second frequency-based analysis approach using a SOM algorithm (Kohonen, 1998) to extract the primary modes of Pacific SSTs within PHYDA without assuming a priori what those modes should be (Methods, Section 2.4). This spatial analysis compliments the NINO index analysis of Figure 3. We use the SOM algorithm to assign annual SST anomaly fields to spatial patterns of a preset number (Figures 4a–4f). Note that because data assimilation relies on the climate model to connect spatial locations, the spatial patterns seen in the SOM analysis reflects the DA prior (though in PHYDA's case, a bias-corrected prior); this is inherent to all data-assimilation-based reconstructions and is the trade-off for dynamical information afforded by the climate model (see Section 2.1).

Figures 4a–4f show the six SOM-derived SST patterns that exist within PHYDA. The percentage-changes shown at the top of each panel indicate the frequency change of each pattern during eruption years compared to all years for SAOD greater than 0.13 (n = 37 eruptions). Referring to Figures 4a and 4b, particularly large shifts occur for SOMs 1 and 2. SOM1 is characterized by a weak El Niño-like warming; the shift in the frequency of this pattern is +104%. In contrast, the frequency of pattern 2, which shows large and intense tropical Pacific warming, decreases by 40%. These conflicting results suggest that there is an increase in the frequency of a muted El Niño-like warming and a decrease in a strong tropical Pacific warming response for eruptions exceeding an SOAD of 0.13.

Figure 4g, box plots indicate whether the percentage frequency changes in panels (a–f) are unusual or indicate a significant departure from randomness. Specifically, panel (g) gives the frequency changes as: $(f_{VOLC} - f_{ALL})/f_{ALL}$, where f_{VOLC} is the frequency of each SOM pattern for eruption years and f_{ALL} the frequency of each SOM pattern for all years (i.e., the fraction of each SOM pattern in the full 2,000-year PHYDA data set). This mean frequency change for each pattern during eruption years is plotted as black crosses in Figure 4g. We did a bootstrap resampling

to test for significance by drawing random years from 1 to 2000 CE with the same sample size as the number of volcanic eruptions, and computing the SOM frequency changes for these samples. We repeated this process 1,000 times and show the distribution of these frequency changes as cyan boxplots in Figure 4g. We performed a similar bootstrap resampling for the age-perturbed ensemble of volcanic event dates, shown as purple boxplots (see Sections 2.5 and 2.6). The results in Figure 4g show that, while patterns 1, 2, and 6 are unusual with respect to the normal range of SOM frequencies and show larger shifts, the shifts do not exceed plausible shifts observed in a resampling of the full time series. Notably, however, the change in pattern 1 does graze the 95% whisker of the bootstrap uncertainty distribution. For the scenarios assuming maximum age uncertainty, patterns 1, 2, and 6 no longer stand out as unusual (comparing black crosses to purple boxplots).

We computed this result for two other volcanic forcing thresholds, SAOD > 0.07, 0.22 (Figures S9 and S10 in Supporting Information S1). For SAOD > 0.07, which contains a larger sample size of eruptions, the shift in pattern 1 is significant compared to the background, but not compared to the age-perturbed ensemble (Figure S9g in Supporting Information S1). In general, the results are consistent across the different volcanic forcing thresholds. Noting that the SOM SST patterns are held constant (as in Figures 4a–4f) for all of the six-pattern SOM results (Figures S9 and S10 in Supporting Information S1), the frequency of pattern 1 (weak El Niño-like warming) increases for all three volcanic forcing thresholds. For the largest class of eruptions (SAOD > 0.22, Figure S10 in Supporting Information S1), the frequency of SOMs 3 and 6, which show a La Niña-like cooling response, both decrease. None of these frequency shifts fully exceed the uncertainty range comparing the shifts to all years and to the age-perturbed ensemble, broadly consistent with the results shown in Figure 4g.

Finally, to check the sensitivity of our results to the number of SOM patterns, we recomputed the SOM frequency changes using four and eight patterns rather than six, using volcanic forcing thresholds of SAOD > 0.07, 0.13, 0.22 (Figures S11–S16 in Supporting Information S1). Note that the order/position of the SOM patterns is not fixed across all SOM computations and changing the number of patterns results in slightly different patterns as determined by the SOM algorithm (e.g., pattern 4 for the 4-SOM analysis resembles pattern 1 for the 6-SOM analysis). Consistent with the six-pattern results, the weak El Niño-like warming pattern for the 4-SOM maps (SOM4, Figures S11–S13 in Supporting Information S1) increases in frequency, and the strong warming mode (SOM2) decreases in frequency. Similarly, using eight patterns (Figures S14–S16 in Supporting Information S1), two weak El Niño-like warming patterns (SOM1, SOM3) increase in frequency, while the La Niña-like pattern (SOM8) and intense tropical Pacific warming pattern (SOM2) decrease in frequency. For SAOD > 0.22, the SOM3 (El Niño-like warming pattern) shift exceeds the uncertainty range for the bootstrap resampling range, but not the age model ensemble.

Taken altogether, the broad similarities in these results suggest that the frequency shifts are robust, even considering different numbers of SOM patterns and different volcanic forcing thresholds. The result of a weak El Niño-like warming response is consistent with modeling studies that suggest warming in the central and eastern tropical Pacific following sufficiently explosive tropical volcanism in the last millennium (Adams et al., 2003; Emile-Geay et al., 2008; Handler, 1984; Khodri et al., 2017; Maher et al., 2015; Pausata et al., 2015, 2016; Stevenson et al., 2016). Importantly, however, while the shifts toward El Niño-like conditions are unusual and consistent across eruption size and SOM pattern number, most do not exceed the 95th percentile of background frequency shifts indicated by resampling tests for all years and within the age-perturbed volcanic forcing years.

4. Discussion

An array of recent GCM simulations support a dynamical connection between volcanism and ENSO. The robust El Niño-like response to volcanism observed in coupled climate model simulations (Adams et al., 2003; Emile-Geay et al., 2008; Handler, 1984; Khodri et al., 2017; Maher et al., 2015; Pausata et al., 2015, 2016; Stevenson et al., 2016) requires independent support from the paleoclimate (observational) record. However, it is difficult to (a) ground model simulations using paleoclimate data and (b) either verify or refute the dynamical hypotheses that may explain this relationship without a broader, subannually resolved, and systematically screened pool of paleoclimate records. To address this, we evaluated a novel data-assimilation-based reconstruction of the last millennium (PHYDA) to check the expression of volcanic forcing on tropical Pacific dynamics, performing a simple hypothesis test.

We find that PHYDA does show a weak El Niño-like warming response, especially in the central equatorial Pacific, following sufficiently large volcanic events, a result that is especially apparent in frequency-based analyses (Figures 3 and 4). The SEA maps indicate weak, statistically insignificant warming in the eruption year (Figure 2), to a much lesser degree than what models show (0.1°C–0.2°C compared to 1°C; see Figure S6 in Supporting Information S1); furthermore, for stronger eruptions, SEA suggests widespread cooling across the tropical Pacific (Figures S2, S3, and S5–S8 in Supporting Information S1). Using a block-bootstrap resampling test, we find that the warming that emerges from the SEA is not significant at the 95% level. The frequency-based analyses, PDFs and SOMs, show an increase in warm SST values in the year of the eruption, and subsequent cooling in years 1 and 2. We used SOMs to isolate patterns of individual SST patterns and then track their frequency after volcanic eruptions. The SOM analysis not only suggests a shift toward weak El Niño-like warming (Figures 4a and 4g) but *also* supports a decrease in the frequency of higher-magnitude tropical Pacific warming events (e.g., Figure 4b). The SOM changes do not categorically trend toward El Niño-like conditions. This result holds across several radiative forcing thresholds (Figures S11–S13 in Supporting Information S1) and SOM pattern numbers (Figures S13–S18 in Supporting Information S1). As mentioned in Section 3, the shifts in the post-eruption year PDFs are significant at the 95% level. Shifts in the SOM pattern frequencies do not exceed uncertainty bounds at the 95% level, with the notable exceptions of SOM1 for SAOD exceeding 0.07 (Figure S9 in Supporting Information S1, 6-SOMs) and SOM3 for SAOD exceeding 0.22 (Figure S16 in Supporting Information S1, 8-SOMs). Uncertainty quantification was performed by resampling the background frequency shifts for all years and age-perturbed volcanic forcing years.

The differences between the SEA, PDF, and SOM results underscore the sensitivity of our conclusions, and the conclusions of many other studies, to analysis method selection. Frequency-sensitive analyses (PDFs, SOM) show evidence of unusual weak El Niño-like warming compared to a background distribution, but composite averaging methods (SEA) do not. It is possible that the frequency-based analyses more effectively filter out climate system noise unrelated to ENSO. SOMs (as well as simple PDFs, Figure 3) employ frequency analysis, whereas SEA uses strictly composite averaging without evaluation of changes in event frequency. Frequency analysis may provide a more robust (or sensitive) analysis method for this type of problem, which depends on event lead-lag relationships; SEA's simplistic composite averaging potentially dampens or obfuscates the true climate signal in the data and may not be sensitive enough for small sample problems like volcanic eruptions over the last millennium. Indeed, the warming is weak enough that it may prove difficult to detect in other data products, such as regional or local paleoclimate reconstructions (especially if SEA is employed).

A consistent strong tropical Pacific warming response to volcanism, as observed in GCMs, does not emerge in PHYDA, which provides an annually resolved NIÑO34 reconstruction spanning two millennia (1–2000 CE), longer than most studies which have historically only evaluated the last 1,000 years. While a weak "El Niño-like" SST pattern increases in frequency following volcanic eruptions in PHYDA, it is possible that a more diverse array of SST responses occur (e.g., Figure 4b); and, as mentioned above, the response is not significant at the 95% level. Furthermore, all our results (both compositing and frequency based) suggest more modest warming in PHYDA compared to GCMs, which simulate a volcanic response which is an order of ga.

A number of recent studies have suggested an oversensitivity of GCM responses to volcanic forcing (e.g. Dee et al., 2020). For example, CMIP5 models (including CESM) tend to overestimate tropospheric cooling following eruptions in the nineteenth and twentieth century (Chylek et al., 2020) and do not correctly capture the observed strengthening of the Northern Hemisphere polar vortex and positive phase NAO conditions (Driscoll et al., 2012); in AMIP5 models, the precipitation response to volcanism is overestimated (Meyer et al., 2016). To illustrate the mismatch, Figure S6 in Supporting Information S1 compares the volcanic SEA of the PHYDA versus CESM-LME NINO34 region SST anomalies. In agreement with the results presented in Dee et al. (2020), the climate model response to volcanic forcing is amplified compared to PHYDA and other paleoclimate proxy records. This comparison alongside other studies call into question the ability of GCMs to correctly simulate the regional climate response to external forcing. To date, however, none of the above-cited GCM analyses have employed SOMs or similar analyses. A more direct DA-GCM requires the evaluation of SOM patterns and amplitudes in CESM and CMIP5-6 models.

Explanations for the model–data mismatch may include an oversensitivity of the GCMs to stratospheric aerosol forcing (LeGrande et al., 2016), structural GCM errors, or uncertainties in the volcanic forcing reconstructions (Stevenson et al., 2016). In particular, the methodology for most volcanic forcing reconstructions is such that ice

core-derived sulfate aerosol loading estimates are scaled to the radiative aerosol forcing observed via satellite retrievals for the 1991 eruption of Pinatubo (Gao et al., 2006; Sigl et al., 2015). If sulfur emissions vary significantly among eruptions, the scaling applied to the volcanic aerosol forcing may harbor large uncertainties and result in forcing that is too large (LeGrande et al., 2016). Finally, recent work demonstrates that the seasonality of volcanic eruptions matters (Stevenson et al., 2017); yet, the ice core reconstructions employed in this work cannot capture the timing of each eruption during the year (unless it is independently deduced from historical documentation). GCM simulations spanning the last millennium assume that all eruptions occur in a single season (Gao et al., 2006; Stevenson et al., 2016). In PHYDA, the beginning of the year is set to April, such that the annual response to volcanism averages over the period April to the following March. It is therefore likely that our data–model comparison inferences are contingent on better constraints on eruption season and implementation of that timing in climate model simulations. Because of the strong seasonality of ENSO, further investigation into the seasonality of the eruption may lend insight to the model–data mismatch.

We note several additional caveats this work. Sample sizes for eruptions exceeding higher thresholds (e.g., larger than Pinatubo) are small. Our analyses average over a small sample size, which likely impacts the robustness of our results. This analysis is further complicated by the fact that the climatic effects of volcanic eruptions are short lived (1–5 years). Because the climatic timescale of response to volcanism is essentially the same as the timescale of ENSO phasing, natural variability confounds our assessment the climate response to external forcing alone. Furthermore, a significant fraction of the global dynamical response to volcanism can map onto ENSO-driven climate change and masquerade as ENSO when it is not, and this is a complicated signal to tease apart; for example, most large eruptions of the twentieth century happened to coincide with El Niño events which counteracted volcanic cooling (Lehner et al., 2016).

Our results are dependent upon accurate dating of the volcanic forcing. We show that under maximum dating uncertainty scenarios, it is very difficult to investigate the climate of short-lived events like eruptions. For example, in our age model scenarios, we see a large increase in the spread of the SOM frequency null, as shown in Figure 4 and Figures S9–S16 in Supporting Information S1. Even with a simulated stochastic shift of $\pm$1–2 years, our ability to detect a volcanic signal is degraded.

Finally, CESM-LME is the prior for PHYDA, and several studies have highlighted the exaggerated ENSO pattern in the CESM model in general. Given that the covariance structure of the climate patterns in PHYDA are dependent on CESM, the patterns produced by the SEA and SOM analyses will by definition include spatial information from CESM. Model biases, in particular in response to volcanic eruptions, may play a role in determining how proxy data are assimilated and expressed in DA reconstructions (e.g., Sanchez et al., 2021). ENSO variance in the model exceeds that of the observations, and this enhanced ENSO response may amplify interactions with volcanic cooling (Stevenson et al., 2016). Even though PHYDA's SSTs have been bias corrected and thus its ENSO spectra is much more similar to observations than the stand-alone CESM-LME (Steiger et al., 2019), the strong volcanic reaction in CESM may still incorrectly bias PHYDA's volcanic response. However, because PHYDA uses an off-line data assimilation approach, its time history is informed only by proxy information. This is important given the fact that the frequency analyses (PDFs and SOMs) shown in Figures 3 and 4 focus on temporal shifts rather than the explicit shape of the pattern of the El Niño SSTs. This, in conjunction with the bias correcting of PHYDA, make it very likely that PHYDA's ENSO is less biased than climate model simulations and is therefore useful in the analyses presented here.

To this point, we assert issues with the magnitude of the tropical Pacific SST response, potentially biased by the prior, would matter more for SEA. The bias in CESM's response to volcanism would lead to an exaggerated El Niño-like response in PHYDA; yet, the warming is not significant in the SEA (Figure 2 and Figures S5 and S6 in Supporting Information S1), nor in the SOM shifts (Figure 4). While the volcanic forcing applied in CESM is different from the volcanic forcing employed here (evolv2k; Toohey & Sigl, 2017), the proxy-specific temporal response to volcanic forcing afforded by PHYDA is distinct from CESM in terms of both time and magnitude. Put another way, CESM's volcanic response, though perhaps overestimated (Dee et al., 2020), does not tip the balance pushing the PHYDA reconstruction to a significant volcanic response. Future work could employ fixed-proxy networks in the DA or use a different climate model or observational prior (i.e., reanalysis) to fully evaluate the impact of the CESM prior on our results.

5. Conclusions

We are left with a few key questions: are volcanic forcing impacts on ENSO detectable in currently available proxy networks and paleoclimate reconstructions? Are we using the correct methods and thresholds for detection? The analysis presented here favors the appearance of weak El Niño-like warming, which (a) may not emerge beyond the noise of internal variability and (b) may be difficult to detect in the paleoclimate proxy record (annually resolved proxy records such as corals intersecting volcanic eruptions lack full tropical Pacific coverage in space and time). Furthermore, a strong, significant cooling signal appears in PDF analyses in years 1 and 2. The SEA and frequency-based results underscore a competition between simplistic averaging methods (SEA), which yields a null result (volcanic eruptions do not significantly change tropical Pacific SSTs in a reliable, predictable way), and two frequency analyses, PDFs and SOMs, which show a similar El Niño-like warming response *and* a La Niña-like cooling response. Frequency analyses may be more sensitive to shifts in ENSO state within the context of small numbers of events. Historically, because of the available time series data, SEA has been employed to ensure consistent comparisons between GCM and paleoclimate data. With forthcoming paleoclimate DA reconstructions, comparisons between gridded model simulations and DA reconstructions may further elucidate the tropical Pacific response to volcanic forcing, enhancing our understanding of the model–data mismatch and improving model forcing and physics.

Indeed, forthcoming paleoclimate data assimilation products may help resolve competing theories regarding the ENSO response to volcanic eruptions (Section 1); however, we assert that such resolution would require DA products which reconstruct ocean dynamical fields, such as circulation, thermocline depth, and potentially surface wind fields. Skillful reconstructions of these ENSO-relevant variables are required to further evaluate the competing influences of the ocean dynamical thermostat (Clement et al., 1996) or Walker Circulation changes driven by remote forcing (Khodri et al., 2017). However, some model-generated hypotheses, such as changes in land–ocean temperature gradients (Ohba et al., 2013; Predybaylo et al., 2017) and ITCZ shifts (Pausata et al., 2020) could be readily evaluated in currently available DA reconstructions (e.g., PHYDA, LMR).

The ability of state-of-the-art GCMs to faithfully simulate ENSO's response to external forcing is of paramount importance to climate prediction as we accelerate into a future with higher anthropogenic greenhouse gas emissions. Furthermore, large volcanic eruptions may occur at any time, with documented impacts on temperature and hydroclimate, but poorly constrained interactions with ENSO. While there is high confidence that ENSO itself will continue under global warming, we have low confidence as to its response to increasing greenhouse gases and other forcings (IPCC, 2013). ENSO's response to continued greenhouse gas forcing, which now exceeds +3 W/m^2 year (exceeding most volcanic forcing events of the Common Era), is made uncertain by the potential for future regime changes, which may manifest as a nonlinear, abrupt shift in response to a linear radiative forcing (Cobb et al., 2003, 2013). It is of global importance to investigate how ENSO will respond to future radiative forcing: ensuring that model simulations and the paleoclimate record, enhanced by data assimilation, can be reconciled is a step toward predicting that response.

Conflict of Interest

The authors declare no conflicts of interest relevant to this study.

Data Availability Statement

All of the code and data used to produce this work are publicly available at https://doi.org/10.5281/zenodo.1198817 and in the Supporting Information of Toohey and Sigl (2017): https://www.earth-syst-sci-data.net/9/809/2017/. The CESM-LME is available via https://www.earthsystemgrid.org/dataset/ucar.cgd.ccsm4.cesmLME.html.

Acknowledgments
This work was supported by Rice University, the University of Texas at Austin Institute for Geophysics Postdoctoral Fellowship (S. Dee), the Institute at Brown for Environment and Society's Voss postdoctoral fellowship (S. Dee), and NOAA-OOM Award NA18OAR4310427 awarded to S. Dee. N. Steiger was supported in part by NSF award 1805490 and in part by ISF award 2654/20.

References

Adams, B. J., Mann, M. E., & Ammann, C. M. (2003). Proxy evidence for an El Nino-like response to volcanic forcing. *Nature*, *426*(6964), 274–278. https://doi.org/10.1038/nature02101

Anchukaitis, K., Buckley, B., Cook, E., Cook, B., D'Arrigo, R., & Ammann, C. (2010). Influence of volcanic eruptions on the climate of the Asian monsoon region. *Geophysical Research Letters*, *37*, L22703. https://doi.org/10.1029/2010GL044843

Angell, J. K. (1988). Impact of El Niño on the delineation of tropospheric cooling due to volcanic eruptions. *Journal of Geophysical Research*, *93*(D4), 3697. https://doi.org/10.1029/JD093iD04p03697

Angell, J. K., & Korshover, J. (1985). Surface temperature changes following the six major volcanic episodes between 1780 and 1980. *Journal of Climate and Applied Meteorology*, *24*(9), 937–951. https://doi.org/10.1175/1520-0450(1985)024<0937:STCFTS>2.0.CO;2

Capotondi, A., Wittenberg, A. T., Newman, M., Di Lorenzo, E., Yu, J.-Y., Braconnot, P., et al. (2015). Understanding ENSO diversity. *Bulletin of the American Meteorological Society*, *96*(6), 921–938. https://doi.org/10.1175/BAMS-D-13-00117.1

Church, J. A., White, N. J., & Arblaster, J. M. (2005). Significant decadal-scale impact of volcanic eruptions on sea level and ocean heat content. *Nature*, *438*(7064), 74–77. https://doi.org/10.1038/nature04237

Chylek, P., Folland, C., Klett, J. D., & Dubey, M. K. (2020). CMIP5 climate models overestimate cooling by volcanic aerosols. *Geophysical Research Letters*, *47*, e2020GL087047. https://doi.org/10.1029/2020GL087047

Clement, A. C., Seager, R., Cane, M. A., & Zebiak, S. E. (1996). An ocean dynamical thermostat. *Journal of Climate*, *9*(9), 2190–2196. https://doi.org/10.1175/1520-0442(1996)009<2190:AODT>2.0.CO;2

Cobb, K. M., Charles, C. D., Cheng, H., & Edwards, R. L. (2003). El Niño/Southern Oscillation and tropical Pacific climate during the last millennium. *Nature*, *424*, 271–276. https://doi.org/10.1038/nature01779

Cobb, K. M., Westphal, N., Sayani, H. R., Watson, J. T., Di Lorenzo, E., Cheng, H., et al. (2013). Highly variable El Niño–Southern Oscillation throughout the Holocene. *Science*, *339*(6115), 67–70. https://doi.org/10.1126/science.1228246

Comboul, M., Emile-Geay, J., Evans, M. N., Mirnateghi, N., Cobb, K. M., & Thompson, D. M. (2014). A probabilistic model of chronological errors in layer-counted climate proxies: Applications to annually banded coral archives. *Climate of the Past*, *10*(2), 825–841.

Dee, S. G., Cobb, K. M., Emile-Geay, J., Ault, T. R., Edwards, R. L., Cheng, H., & Charles, C. D. (2020). No consistent ENSO response to volcanic forcing over the last millennium. *Science*, *367*(6485), 1477–1481. https://doi.org/10.1126/science.aax2000

Driscoll, S., Bozzo, A., Gray, L. J., Robock, A., & Stenchikov, G. (2012). Coupled Model Intercomparison Project 5 (CMIP5) simulations of climate following volcanic eruptions. *Journal of Geophysical Research*, *117*, D17105. https://doi.org/10.1029/2012JD017607

Emile-Geay, J., Cobb, K. M., Cole, J. E., Elliot, M., & Zhu, F. (2020). Past ENSO variability: Reconstructions, models, and implications. In *El Niño Southern Oscillation in a changing climate* (pp. 87–118).

Emile-Geay, J., Seager, R., Cane, M. A., Cook, E. R., & Haug, G. H. (2008). Volcanoes and ENSO over the past millennium. *Journal of Climate*, *21*(13), 3134–3148. https://doi.org/10.1175/2007JCLI1884.1

Gao, C., Robock, A., Self, S., Witter, J. B., Steffenson, J., Clausen, H. B., et al. (2006). The 1452 or 1453 A.D. Kuwae eruption signal derived from multiple ice core records: Greatest volcanic sulfate event of the past 700 years. *Journal of Geophysical Research*, *111*, D12107. https://doi.org/10.1029/2005JD006710

Gleckler, P. J., Wigley, T. M. L., Santer, B. D., Gregory, J. M., Achutarao, K., & Taylor, K. E. (2006). Volcanoes and climate: Krakatoa's signature persists in the ocean. *Nature*, *439*(7077), 675. https://doi.org/10.1038/439675a

Handler, P. (1984). Possible association of stratospheric aerosols and El Niño type events. *Geophysical Research Letters*, *11*(11), 1121–1124. https://doi.org/10.1029/GL011i011p01121

Handler, P., & Andsager, K. (1994). El Niño, volcanism, and global climate. *Human Ecology*, *22*(1), 37–57. https://doi.org/10.1007/bf02168762

Horton, D. E., Johnson, N. C., Singh, D., Swain, D. L., Rajaratnam, B., & Diffenbaugh, N. S. (2015). Contribution of changes in atmospheric circulation patterns to extreme temperature trends. *Nature*, *522*(7557), 465. https://doi.org/10.1038/nature14550

IPCC. (2013). Summary for policymakers. In *SPM* (pp. 1–30). Cambridge, United Kingdom/New York: Cambridge University Press. https://doi.org/10.1017/CBO9781107415324.004

Johnson, N. C. (2013). How many ENSO flavors can we distinguish? *Journal of Climate*, *26*(13), 4816–4827. https://doi.org/10.1175/JCLI-D-12-00649.1

Johnson, N. C., Feldstein, S. B., & Tremblay, B. (2008). The continuum of northern hemisphere teleconnection patterns and a description of the NAO shift with the use of self-organizing maps. *Journal of Climate*, *21*(23), 6354–6371. https://doi.org/10.1175/2008JCLI2380.1

Kay, J. E., Deser, C., Phillips, A., Mai, A., Hannay, C., Strand, G., et al. (2015). The Community Earth System Model (CESM) large ensemble project: A community resource for studying climate change in the presence of internal climate variability. *Bulletin of the American Meteorological Society*, *96*(8), 1333–1349. https://doi.org/10.1175/BAMS-D-13-00255.1

Khodri, M., Izumo, T., Vialard, J., Janicot, S., Cassou, C., Lengaigne, M., et al. (2017). Tropical explosive volcanic eruptions can trigger El Niño by cooling tropical Africa. *Nature Communications*, *8*(1), 778. https://doi.org/10.1038/s41467-017-00755-6

Kohonen, T. (1998). The self-organizing map. *Neurocomputing*, *21*(1), 1–6. https://doi.org/10.1016/S0925-2312(98)00030-7

LeGrande, A. N., Tsigaridis, K., & Bauer, S. E. (2016). Role of atmospheric chemistry in the climate impacts of stratospheric volcanic injections. *Nature Geoscience*, *9*, 652–655. https://doi.org/10.1038/ngeo2771

Lehner, F., Schurer, A. P., Hegerl, G. C., Deser, C., & Frölicher, T. L. (2016). The importance of ENSO phase during volcanic eruptions for detection and attribution. *Geophysical Research Letters*, *43*, 2851–2858. https://doi.org/10.1002/2016GL067935

Li, J., Xie, S.-P., Cook, E. R., Morales, M. S., Christie, D. A., Johnson, N. C., et al. (2013). El Niño modulations over the past seven centuries. *Nature Climate Change*, *3*(9), 822–826. https://doi.org/10.1038/nclimate1936

Maher, N., McGregor, S., England, M. H., & Gupta, A. S. (2015). Effects of volcanism on tropical variability. *Geophysical Research Letters*, *42*, 6024–6033. https://doi.org/10.1002/2015GL064751

Mann, M. E., Cane, M. A., Zebiak, S. E., & Clement, A. (2005). Volcanic and solar forcing of the tropical Pacific over the past 1000 years. *Journal of Climate*, *18*(3), 447–456. https://doi.org/10.1175/JCLI-3276.1

McCormick, M. P., Thomason, L. W., & Trepte, C. R. (1995). Atmospheric effects of the Mt Pinatubo eruption. *Nature*, *373*, 399–404. https://doi.org/10.1038/373399a0

McGregor, S., & Timmermann, A. (2011). The effect of explosive tropical volcanism on ENSO. *Journal of Climate*, *24*(8), 2178–2191. https://doi.org/10.1175/2010JCLI3990.1

Meyer, A., Folini, D., Lohmann, U., & Peter, T. (2016). Tropical temperature and precipitation responses to large volcanic eruptions: Observations and AMIP5 simulations. *Journal of Climate*, *29*(4), 1325–1338.

Ohba, M., Shiogama, H., Yokohata, T., & Watanabe, M. (2013). Impact of strong tropical volcanic eruptions on ENSO simulated in a coupled GCM. *Journal of Climate*, *26*(14), 5169–5182. https://doi.org/10.1175/JCLI-D-12-00471.1

Pausata, F. S., Chafik, L., Caballero, R., & Battisti, D. S. (2015). Impacts of high-latitude volcanic eruptions on ENSO and AMOC. *Proceedings of the National Academy of Sciences of the United States of America*, *112*(45), 784–788. https://doi.org/10.1073/pnas.1509153112

Pausata, F. S., Karamperidou, C., Caballero, R., & Battisti, D. S. (2016). ENSO response to high-latitude volcanic eruptions in the northern hemisphere: The role of the initial conditions. *Geophysical Research Letters*, *43*, 8694–8702. https://doi.org/10.1002/2016GL069575

Pausata, F. S., Zanchettin, D., Karamperidou, C., Caballero, R., & Battisti, D. S. (2020). ITCZ shift and extratropical teleconnections drive ENSO response to volcanic eruptions. *Science Advances*, *6*(23), eaaz5006. https://doi.org/10.1126/sciadv.aaz5006

Predybaylo, E., Stenchikov, G. L., Wittenberg, A. T., & Zeng, F. (2017). Impacts of a Pinatubo-size volcanic eruption on ENSO. *Journal of Geophysical Research: Atmospheres*, *122*, 925–947. https://doi.org/10.1002/2016JD025796

Robock, A. (2000). Volcanic eruptions and climate. *Reviews of Geophysics*, *38*(2), 191–219. https://doi.org/10.1029/1998RG000054

Robock, A., & Mao, J. (1995). The volcanic signal in surface temperature observations. *Journal of Climate*, *8*(5), 1086–1103. https://doi.org/10.1175/1520-0442(1995)008<1086:TVSIST>2.0.CO;2

Sanchez, S. C., Hakim, G. J., & Saenger, C. P. (2021). Climate model teleconnection patterns govern the Niño-3.4 response to early nineteenth-century volcanism in coral-based data assimilation reconstructions. *Journal of Climate*, *34*(5), 1863–1880. https://doi.org/10.1175/JCLI-D-20-0549.1

Shindell, D. T., & Schmidt, G. A. (2004). Dynamic winter climate response to large tropical volcanic eruptions since 1600. *Journal of Geophysical Research*, *109*, D05104. https://doi.org/10.1029/2003JD004151

Shindell, D. T., Schmidt, G. A., Miller, R. L., & Mann, M. E. (2003). Volcanic and solar forcing of climate change during the preindustrial era. *Journal of Climate*, *16*, 4094–4107. https://doi.org/10.1175/1520-0442(2003)016<4094:VASFOC>2.0.CO;2

Sigl, M., Winstrup, M., McConnell, J. R., Welten, K. C., Plunkett, G., Ludlow, F., et al. (2015). Timing and climate forcing of volcanic eruptions for the past 2,500 years. *Nature*, *523*(7562), 543–549. https://doi.org/10.1038/nature14565

Steiger, N. J., Smerdon, J. E., Cook, B. I., Seager, R., Williams, A. P., & Cook, E. R. (2019). Oceanic and radiative forcing of medieval megadroughts in the American Southwest. *Science Advances*, *5*(7), eaax0087. https://doi.org/10.1126/sciadv.aax0087

Steiger, N. J., Smerdon, J. E., Cook, E. R., & Cook, B. I. (2018). A reconstruction of global hydroclimate and dynamical variables over the Common Era. *Scientific Data*, *5*, 180–086. https://doi.org/10.1038/sdata.2018.86

Stevenson, S., Fasullo, J. T., Otto-Bliesner, B. L., Tomas, R. A., & Gao, C. (2017). Role of eruption season in reconciling model and proxy responses to tropical volcanism. *Proceedings of the National Academy of Sciences of the United States of America*, *114*(8), 1822–1826. https://doi.org/10.1073/pnas.1612505114

Stevenson, S., Otto-Bliesner, B., Fasullo, J., & Brady, E. (2016). 'El Niño like' hydroclimate responses to last millennium volcanic eruptions. *Journal of Climate*, *29*(8), 2907–2921. https://doi.org/10.1175/JCLI-D-15-0239.1

Tardif, R., Hakim, G. J., Perkins, W. A., Horlick, K. A., Erb, M. P., Emile-Geay, J., et al. (2019). Last millennium reanalysis with an expanded proxy database and seasonal proxy modeling. *Climate of the Past*, *15*(4), 1251–1273. https://doi.org/10.5194/cp-15-1251-2019

Tejedor, E., Steiger, N., Smerdon, J., Serrano-Notivoli, R., & Vuille, M. (2021b). Global temperature responses to large tropical volcanic eruptions in paleo data assimilation products and climate model simulations over the last millennium. *Paleoceanography and Paleoclimatology*, *36*, e2020PA004128. https://doi.org/10.1029/2020PA004128

Tejedor, E., Steiger, N. J., Smerdon, J. E., Serrano-Notivoli, R., & Vuille, M. (2021a). Global hydroclimatic response to tropical volcanic eruptions over the last millennium. *Proceedings of the National Academy of Sciences of the United States of America*, *118*(12), e2019145118. https://doi.org/10.1073/pnas.2019145118

Timmreck, C. (2012). Modeling the climatic effects of large explosive volcanic eruptions. *Wiley Interdisciplinary Reviews: Climate Change*, *3*(6), 545–564. https://doi.org/10.1002/wcc.192

Toohey, M., & Sigl, M. (2017). Volcanic stratospheric sulfur injections and aerosol optical depth from 500 BCE to 1900 CE. *Earth System Science Data Discussions*, *9*, 809–831.

Zhu, F., Emile-Geay, J., Anchukaitis, K. J., Hakim, G. J., Wittenberg, A. T., Morales, M. S., et al. (2022). A re-appraisal of the ENSO response to volcanism with paleoclimate data assimilation. *Nature Communications*, *13*, 747.

Zhu, F., Emile-Geay, J., Hakim, G. J., King, J., & Anchukaitis, K. J. (2020). Resolving the differences in the simulated and reconstructed temperature response to volcanism. *Geophysical Research Letters*, *47*, e2019GL086908. https://doi.org/10.1029/2019GL086908